Cardiovascular safety of fenfluramine in the treatment of Dravet syndrome: Analysis of an ongoing long-term open-label safety extension study

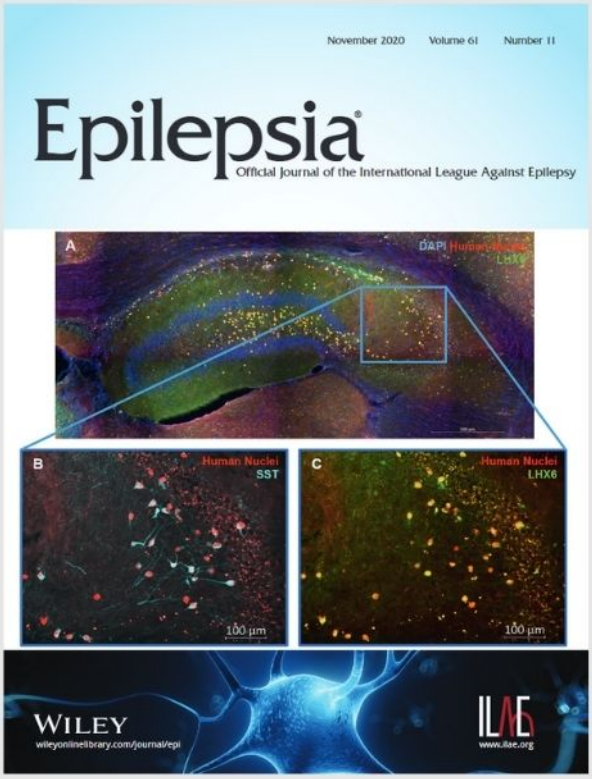

Discover this research article in full today.

View enhanced article features, including:

- **full article audio recording**
- **video abstract**
- **author discussion**
- **infographic**

Received: 19 January 2023 | Revised: 19 April 2023 | Accepted: 2 May 2023

DOI: 10.1002/hbm.26344

RESEARCH ARTICLE

WILEY

Spatial–temporal patterns of brain disconnectome in Alzheimer's disease

Li Liang[1] | Pengzheng Zhou[2] | Chenfei Ye[3] | Qi Yang[4] | Ting Ma[1,2,3,5]

[1]Department of Electronic & Information Engineering, Harbin Institute of Technology (Shenzhen), Shenzhen, China

[2]Peng Cheng Laboratory, Shenzhen, Guangdong, China

[3]International Research Institute for Artificial Intelligence, Harbin Institute of Technology (Shenzhen), Shenzhen, China

[4]Department of Radiology, Beijing Chao-Yang Hospital, Capital Medical University, Beijing, China

[5]Guangdong Provincial Key Laboratory of Aerospace Communication and Networking Technology, Harbin Institute of Technology (Shenzhen), Shenzhen, China

Correspondence
Ting Ma, Department of Electronic & Information Engineering, Harbin Institute of Technology (ShenZhen), Rm 1206, Information Building, HIT Campus, Shenzhen University Town, Nanshan District, Shenzhen, Guangdong Province, 518055, China.
Email: tma@hit.edu.cn

Funding information
Basic Research Foundation of Shenzhen Science and Technology Stable Support Program, Grant/Award Number: GXWD20201230155427003-20200822115709001; National Natural Science Foundation of China, Grant/Award Numbers: 62276081, 62106113; The Innovation Team and Talents Cultivation Program of National Administration of Traditional Chinese Medicine, Grant/Award Number: NO: ZYYCXTD-C-202004

Abstract

Mounting evidences have shown that progression of white matter hyperintensities (WMHs) with vascular origin might cause cognitive dysfunction symptoms through their effects on brain networks. However, the vulnerability of specific neural connection related to WMHs in Alzheimer's disease (AD) still remains unclear. In this study, we established an atlas-guided computational framework based on brain disconnectome to assess the spatial–temporal patterns of WMH-related structural disconnectivity within a longitudinal investigation. Alzheimer's Disease Neuroimaging Initiative (ADNI) database was adopted with 91, 90 and 44 subjects including in cognitive normal aging, stable and progressive mild cognitive impairment (MCI), respectively. The parcel-wise disconnectome was computed by indirect mapping of individual WMHs onto population-averaged tractography atlas. By performing chi-square test, we discovered a spatial–temporal pattern of brain disconnectome along AD evolution. When applied such pattern as predictor, our models achieved highest mean accuracy of 0.82, mean sensitivity of 0.86, mean specificity of 0.82 and mean area under the receiver operating characteristic curve (AUC) of 0.91 for predicting conversion from MCI to dementia, which outperformed methods utilizing lesion volume as predictors. Our analysis suggests that brain WMH-related structural disconnectome contributes to AD evolution mainly through attacking connections between: (1) parahippocampal gyrus and superior frontal gyrus, orbital gyrus, and lateral occipital cortex; and (2) hippocampus and cingulate gyrus, which are also vulnerable to Aβ and tau confirmed by other researches. All the results further indicate that a synergistic relationship exists between multiple contributors of AD as they attack similar brain connectivity at the prodromal stage of disease.

KEYWORDS

Alzheimer's disease, brain disconnectome, cerebral small vessel disease, mild cognitive impairment, spatial–temporal pattern, white matter hyperintensities

1 | INTRODUCTION

Increasing evidences recognize Alzheimer's disease (AD) as a multifactorial and heterogeneous disease with multiple contributors to its pathophysiology, including cerebral vascular dysfunction (Soto-Rojas et al., 2021; Sweeney et al., 2019). According to the two-hit vascular hypothesis of AD pathology, dysfunction of brain microcirculation initiates a cascade of pathogenetic events that cause regional lesions in brain parenchyma which contribute to dementia through directly damage of neurons and their connectivity (Apátiga-Pérez et al., 2021; Iadecola, 2017; Sweeney et al., 2019). Regional burden of white matter hyperintensities (WMHs) with presumed vascular origin, are typical image markers of cerebral small vessel disease (CSVD), which is a disorder of the brain's small perforating arterioles, capillaries, and probably venules (Wardlaw et al., 2019). Although mounting evidences have confirmed that associations between the presence of WMHs and decreased cognitive functions are, at least in part, mediated through network disruption (Ter Telgte et al., 2018), the question of which specific neural circuits are particularly vulnerable to or suffering the most severe impairments from the accumulation of regional WMHs across the spectrum of AD neurodegeneration still remains unclear.

In recent years, diffusion MRI had been evolved as a powerful method to quantify brain structural connectivity alterations associated with AD. Diffusion alterations in the white matter are frequently observed across the AD continuum (Nasrabady et al., 2018). In presymptomatic sporadic and mutation carriers of autosomal dominant AD, microstructural alterations (fractional anisotropy, FA and mean diffusivity, MD) were observed accompanied with pathological accumulation in anterior cingulum, posterior cingulum, and uncinate fasciculus (Pichet Binette et al., 2021). Studies using regions-of-interest or tract-based analysis detected specific spatial patterns of structural connectivity alterations located in parahippocampal cingulum and inferior temporal in AD and mild cognitive impairment (MCI) cohorts (Raghavan et al., 2022; Vemuri et al., 2019). Using fixel-based analysis with constrained spherical deconvolution (Dhollander et al., 2021), researchers reported reductions in both fiber density and fiber-bundle cross-section of specific fiber pathways associated with default mode network nodes in AD (Mito et al., 2018). Furthermore, reductions of fiber density and cross-section were detected within posterior cingulum in MCI cohorts (Mito et al., 2018).

However, global structural and tract-specific connectivity metrics seem largely determined by CSVD-related white matter damage other than AD biomarkers in a memory clinic setting, even in samples in which AD was the clinically predominant disease (Finsterwalder et al., 2020; Taylor et al., 2016). While AD and CSVD are distinct disease, the majority of patients who seek clinical care in memory clinics present with both AD and CSVD-related brain alterations to varying degrees (Dewenter et al., 2022). A histopathology study found that up to 80% of patients with prodromal AD show cerebrovascular alterations upon autopsy (Kapasi et al., 2017). A widely held view is that CSVD-associated white matter damages are caused by dysfunctions of vascular-glio-neuronal unit including: chronic hypoperfusion, impaired cerebrovascular reactivity, dysfunction of glymphatic system, blood–brain barrier leakage or compromised myelin remodeling (Joutel & Chabriat, 2017; Wardlaw et al., 2019). The vessel-intrinsic mechanisms also contribute to amyloid accumulation through cerebral amyloid angiopathy (Dadar et al., 2020; Lorenzini et al., 2022). These evidences suggest an interactive and synergistic relationship exists between CSVD and AD, which enlighten us to consider the contribution of WMHs while investigating the progressive impairments of structural connectivity associated with AD.

Recently, structural disconnectome has been proposed to characterize the disruptions caused by local lesions on connectivity by spatially mapping white matter fiber tracts with regional brain lesions (Carolyn D. Langen et al., 2017; Zayed et al., 2020). Studies using 3714 participants from Rotterdam Study found that WMH-related disconnectome was especially related to worse executive functioning and concluded that WMH-related disconnectome explains more variation in cognitive function than regional lesion volumes (C. D. Langen et al., 2018).

In this study, we hypothesized that specific neural connections or circuits are preferentially targeted by the progression of regional WMHs in patients of prodromal AD before large-scale brain connectivities are disturbed. As the evolution of AD physiopathology, an inherent spatial–temporal progressive pattern of WMH-related brain structural disconnectome can be detected by neuroimaging at parcel-wise connection level. These knowledges might help us gain a better understanding of how CSVD contributing to AD pathophysiology, and result in better prognosis of neurodegeneration in MCI cohorts. However, to our best knowledge, there is no study focusing on unraveling the progressive patterns of WMH-related structural disconnectome across the spectrum of AD, mainly due to lack of computational methods to associate regional WMH accumulation with disconnections happened between specific pair of brain regions.

To address this caveat, we used well-described brain disconnectome to quantify the disruptions of WMHs exerted on brain structural connectivity, we then established an atlas-guided indirect mapping framework to assess the spatial distinctive and temporal progressive brain disconnectome due to WMHs at parcel-wise connection level using a longitudinal dataset including cognitive normal (CN), stable MCI (sMCI) and progressive MCI (pMCI) groups. Prediction models for conversion from MCI to dementia were proposed. Our results found that specific connections associated with parahippocampal gyrus, and hippocampus are significantly vulnerable to the progression of WMHs in pMCI cohort. We proved that this pattern of brain disconnectome is a promising predictor for AD-related neurodegeneration.

2 | MATERIALS AND METHODS

2.1 | Data preparation

Data used in current study were obtained from the Alzheimer's Disease Neuroimaging Initiative (ADNI) database (adni.loni.usc.edu). The ADNI was launched in 2003 by the National Institute on Aging (NIA),

the National Institute of Biomedical Imaging and Bioengineering (NIBIB), the Food and Drug Administration (FDA), private pharmaceutical companies and non-profit organisations, as a public-private partnership. It has become the largest opensource database for studying progression of MCI and early AD. Three groups with longitudinal follow-up visits were enrolled in this study, including CN, sMCI, and pMCI. The stable MCI are individuals diagnosed as MCI at baseline, but did not convert to dementia during the whole follow-up (at least 3 years). The CN group includes individuals diagnosed as cognitive normal during whole follow-up visits (at least 3 years). The pMCI group includes subjects who diagnosed as MCI at the baseline, and eventually converted to AD at any of the follow-up visits. The inclusion criteria were as follows: First, MRI acquisitions including both T1 weighted and T2-weighted with fluid-attenuated inversion recovery (T2-FLAIR) imaging are available at three longitudinal visits: baseline, the first follow-up and the second follow-up. Second, in pMCI group, the second visit (i.e., the first follow-up) should be at least 1 year before conversion, patients should be diagnosed as dementia at the last visit (i.e., the second follow-up). Third, the age of all the enrolled subjects should be between 65 and 85 years at the baseline. Fourth, neurological assessment batteries including Alzheimer's Disease Assessment Scale (ADAS), and Mini Mental State Examination (MMSE) are available at three visits. MMSE score should be larger than 21 at baseline. Neurological assessments should be in the same year as MRI acquisitions. Last, negative results on amyloid-β status for cognitive normal subjects, positive results on amyloid-β status for subjects in sMCI and pMCI group. The subjects inclusion is summarized in Figure 1.

For further selection, subjects were excluded for following reasons: First, nonmonotone diagnosis. Second, diagnosis not available at the last visit. Third, other pathologies exist, such as stroke, depression and craniocerebral trauma. Fourth, High levels of MR artifacts due to head-motion or magnetic susceptibility distortion, and failure of brain segmentation using T1. As shown in Figure 1, 37 CN subjects and 47 MCI subjects were excluded in this procedure.

Finally, we included 91, 90 and 44 individuals in CN, sMCI and pMCI groups at baseline, respectively. Then we labeled the time point for the last visit based on the conversion diagnosis in pMCI group, time duration between baseline and the last visit of pMCI subjects were 3.20 ± 1.36 years. We further defined the second visit for pMCI group based on the principle that the time should be at least 1 year before conversion. At last, the time of second visit for CN and sMCI was determined according to the duration in pMCI group, respectively. All participants had provided informed written consent before recruitment and filled out questionnaires approved by the respective Institutional Review Board (IRB). The demographic information of enrolled subjects at baseline are shown in Table 2.

2.2 | Image acquisition protocol

Typical MRI scan parameters of T1 are field strength is 3.0 T; flip angle = 9.0°; manufacturer = SIEMENS; matrix: 240 × 256 × 176; pixel spacing $X = 1.0$ mm, $Y = 1.0$ mm; pulse sequence = GR/IR; slice thickness = 1.2 mm; TE = 3.0 ms; TI = 900.0 ms; TR = 2300.0 ms.

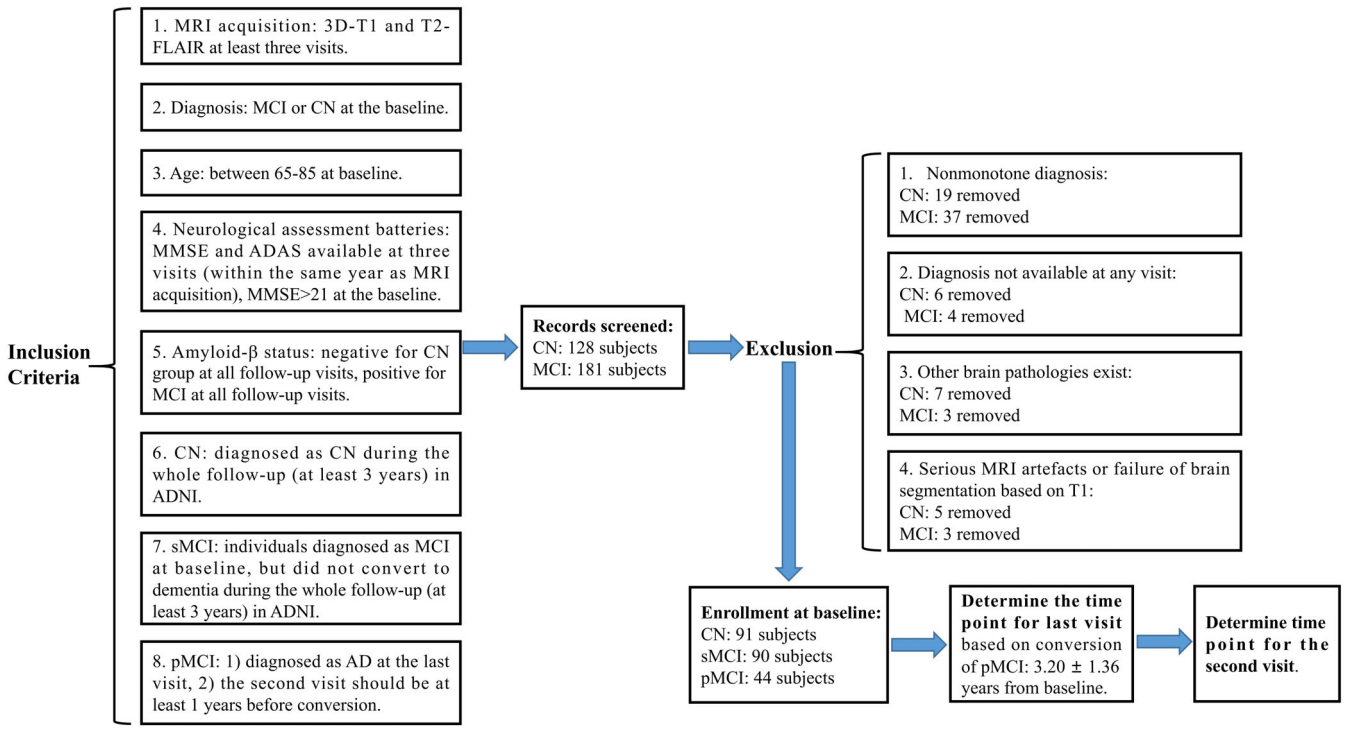

FIGURE 1 Flowchart of subject enrollment and the determination of time point for longitudinal follow-up visits.

Typical MRI scan parameters of T2-FLAIR are acquisition plane = AXIAL; field strength = 3.0 T; flip angle = 150.0°; manufacturer = SIEMENS; matrix: 256 × 256 × 35; pixel spacing $X = 0.9$ mm; pixel spacing $Y = 0.9$ mm; pulse sequence = SE/IR; slice thickness = 5.0 mm; TE = 91.0 ms; TI = 2500.0 ms; TR = 9000.0 ms.

2.3 | Image preprocessing

We performed whole brain parcellation using Brain Label (http://brainsite.cn/), which provides automated cloud service for whole brain tissue parcellation of T1 images based on multiple atlas likelihood fusion algorithm and preselection strategy (Tang et al., 2013; Wu et al., 2016). Brain Label segments the whole brain into 283 regions consisted of gray matter, white matter, cerebrospinal fluid and ventricle. After whole brain parcellation was performed, T1 was transformed to the native space of T2-FLAIR by intrasubject coregistration using FSL FLIRT (Jenkinson et al., 2002; Jenkinson & Smith, 2001) so that brain parcellation can immediately define on T2-FLAIR. We then performed global inhomogeneity corrections of T1 and T2-FLAIR using N4 bias field correction (Tustison et al., 2010) built in advanced normalization tools (ANTs). For following WMH segmentation, we further normalized the intensities of T1 and T2-FLAIR by Gaussian normalization. Intracranial brain tissue mask in the space of T2-FLAIR was generated by FSL BET (Smith, 2002).

2.4 | Modeling brain disconnectome

WMH segmentation was performed using a self-developed deep learning-based pipeline: ^{A}U-Net (Liang et al., 2021; Ronneberger et al., 2015). Two observers independently inspected the quality of WMH segmentation and localization blinded from diagnostic and demographic information. After discussion between two observers, manually corrections were performed for false segmentation and wrongly localization of WMHs. Regional volumes of WMHs in 29 predefined white matter regions (Liang et al., 2021) were calculated then normalized by whole brain white matter volume for further analysis. We also calculated the whole brain WMH volume for each subject, and normalized by whole brain white matter volume.

Atlas-guided indirect mapping method (Carolyn D. Langen et al., 2017) was used to compute brain disconnectome as shown in Figure 2. Binarized WMH lesion maps were warped to Montreal Neurological Institute 1 mm isotropic space (MNI152) through nonlinear coregistration between T1 images using symmetric normalization implemented in ANTs (Avants et al., 2008). We used the population-averaged white matter tractography atlas (HCP842) (Yeh et al., 2018) as streamline template for computing whole brain connectivity (denoted as atlas connectome). Label images produced by brain parcellation were transformed to MNI152 space, then regrouped to 31 gray matter regions (Fan et al., 2016), details are shown in Appendix. This parcellation was used as template for constructing parcel-wise connectome. We calculated the number of streamlines which traversed through the volumes occupied by WMHs (these streamlines are denoted as WMH-affected streamlines). WMH-affected streamlines for each parcel-wise connection were normalized by total streamlines within this connection to obtain parcel-wise disconnectome.

Age and education are known to affect the regional volume of WMHs (Hu et al., 2021; Wardlaw et al., 2019), further associated with WMH-related parcel-wise disconnectome. We adopted the method proposed by Dukart et al. (2011) to correct for the confounding effects induced by age and education. Given that there is no significant group difference between CN, sMCI and pMCI based on age and education in our study (Table 2), we performed multiple linear regression as Equation (1) in CN cohorts.

$$Y_{CN} = \beta_0 + \beta_1 X_{CN,age} + \beta_2 X_{CN,edu} \quad (1)$$

$$Y_{corr} = \max\left((Y - \beta_1 X_{age} - \beta_2 X_{edu}), 0\right) \quad (2)$$

In Equation (1), $X_{CN,age}$ and $X_{CN,edu}$ are the age and education vector for CN subjects. Y_{CN} is the parcel-wise disconnectome associated with CN before correction. After the coefficients: β_1 and β_2 were estimated, they were applied to the whole dataset to obtain corrected parcel-wise disconnectome Y_{corr} as shown in Equation (2).

We further computed binarized residual connectome using the corrected parcel-wise disconnectome as shown in Table 1. Disconnectome progress was defined by Equation (3).

$$DP_{vi} = R_{bs} - R_{vi} \quad (3)$$

R_{vi} represents the binarized residual connectome at the first or second follow-up, corresponding to $vi = 1$ or 2, respectively. R_{bs} denotes binarized residual connectome at baseline. DP represents WMH-related disconnectome progress. For each subject at specific follow-up visit, $DP_{vi} = 1$ indicates progressive disconnection happened between specific pair of regions, whereas $DP_{vi} = 0$ denotes reserving of connection.

2.5 | Prediction models

Prediction models for conversion from MCI to dementia were proposed using three types of classifiers: logistic regression, support vector machine and random forest. These models are built in different time points, which were baseline and the first follow-up. We calculated corrected parcel-wise disconnectome between one gray matter region and the other gray matter regions, resulting in a 31 × 1 feature vector for each subject (hereinafter referred to as node disconnectome). Disconnectome progress was computed by subtracting baseline node disconnectome from the first follow-up node

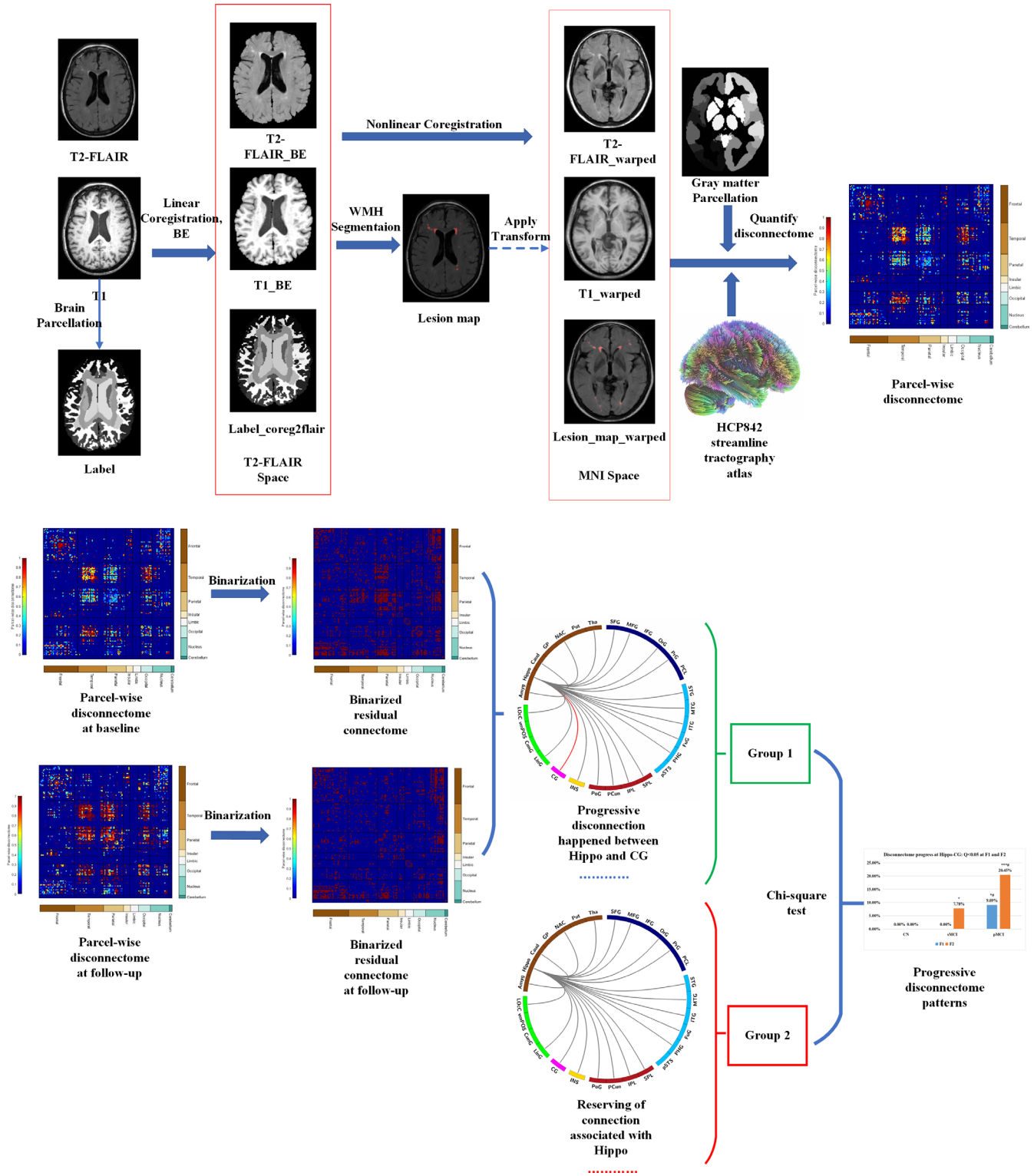

FIGURE 2 Flowchart of atlas-guided indirect mapping framework. BE, brain tissue extraction; coreg2flair, coregister to T2-FLAIR space; CG, cingulate gyrus; Hippo, hippocampus.

disconnectome without binarization in this section, which generating another 31 × 1 feature vector for each subject at the first follow-up (hereinafter referred to as node disconnectome progress). For each type of classifiers, five prediction models were proposed, with two of them at baseline utilizing normalized regional WMH volumes (vector with 29 elements) and node disconnectome; and three of them at the first follow-up utilizing normalized regional WMH volumes (vector with 29 elements), node disconnectome and node disconnectome

TABLE 1 Computing binarized residual connectome.

Connectivity between brain region *i* and *j*	No-connection in atlas	With-connection in atlas	
Streamlines in atlas connectome	=0	>0	>0
Parcel-wise disconnectome	–	>thresh	<thresh
Binarized residual connectome	=0	=0	=1

Abbreviation: thresh, threshold, which was set to 0.5 in this study.

progress. In summary, totally 15 models with different feature sets were proposed as shown in Table 4.

For each prediction model, cross-validation was performed 100 times. In order to tackle the class imbalance problem, in each cross-validation, 44 subjects were randomly chosen from sMCI group (with totally 90 subjects), resulting a subset consisted of 44 sMCI subjects and 44 pMCI subjects. We then performed leave-one-out cross validation in this subset. Sensitivity, specificity, accuracy, receiver operating characteristic curve (ROC) and area under the curve (AUC) were calculated in this subset.

Feature selections associated with LR and SVM were performed by L1 regularization (LASSO) (Tibshirani, 1996). We used "RandomForestClassifier" built in python package "sklearn. ensemble" to construct random forest models, with number of decision trees equals to 36. In order to decide the optimal number of decision trees, we simply performed leave-one-out cross validation in the whole dataset (90 sMCI and 44 pMCI) with a grid search from 1 to 200 decision trees (step = 1), and maximizing the classification accuracy.

2.6 | Statistical analysis

For demographics and neuropsychological sores: group difference associated with gender was detected by chi-square test; group differences associated with age, education, time duration between different visits and neuropsychological scores were detected using non-parametric Kruskal–Wallis test. Post-hoc comparisons were performed by Mann–Whitney *U* test.

We performed group comparison and post-hoc analysis between CN, sMCI and pMCI based on WMH burden (measured by whole brain WMH volume normalized by bilateral cerebellum gray matter volume and parcel-wise disconnnectome) at baseline, using analysis of covariance (ANCOVA) with age and education added as covariates. Furthermore, each subject can be classified into small WMH burden (whole brain WMH volume ≤5 mL), medium WMH burden (5 mL < whole brain WMH volume ≤ 15 mL), and large WMH burden (whole brain WMH volume > 15 mL). We used chi-square test to detect whether there is significant difference based on proportion of different WMH burden group. Chi-square test was used to detect significant disconnectome progress for both group and post-hoc comparisons.

Multiple comparisons were corrected by performing permutation test for 10,000 times, we shuffled our data based on diagnostic groups. Empirical distributions of maximum statistics (*F* for testing group difference associated with parcel-wise disconnectome at baseline, χ^2 for testing group difference associated with disconnectome progress) under null hypothesis were computed. We controlled false discovery rate (α) under 0.05.

We compared the performance of prediction models using node disconnectome and node disconnectome progress with those models using normalized regional WMH volumes by one-tail unpaired *T*-test, where multiple comparisons were corrected by FDR correction (Benjamini & Hochberg, 1995).

3 | RESULTS

3.1 | Demographics and neuropsychological scores

Patients in sMCI and pMCI groups did not differ from cognitive normal controls in age, gender, and education level. As shown in Table 2, significant group differences were detected based on neuropsychological scores. Post-hoc comparison showed no differences between sMCI and pMCI based on neuropsychological scores at baseline. At the first and second follow-up visit, pMCI group had presented significantly larger ADAS scores and lower MMSE scores compared with sMCI group. Time durations between baseline and follow-up visits did not differ among three groups in this study.

3.2 | WMH burden at baseline

As shown in Table 3, neither normalized whole brain WMH volume nor proportion of different WMH burden group presented significant difference between CN, sMCI, and pMCI.

As shown in Figure 3, group comparisons detected significant difference in connection between parahippocampal gyrus and orbital gyrus (PHG-OrG) after performing correction for multiple comparisons. In this connection, pMCI individuals suffered from significant higher brain disconnetome than both sMCI and CN, whereas sMCI cohorts did not differ from CN.

3.3 | Spatial–temporal patterns of brain disconnectome

As shown in Figure 4, we detected progressive disconnections happened in connectivity between parahippocampal gyrus and superior

TABLE 2 Demographics and neuropsychological scores.

Demographics and neuropsychological scores	CN	sMCI	pMCI
Gender (Male/Female)	43/48	44/46	24/20
Age (years)	74.02 ± 7.13	74.35 ± 7.09	75.18 ± 8.16
Education (years)	16.30 ± 2.44	16.26 ± 2.13	16.33 ± 2.58
Time duration between baseline and first follow-up (in years)	1.07 ± 0.20	1.10 ± 0.14	1.14 ± 0.32
Time duration between baseline and second follow-up (in years)	3.38 ± 0.97	3.32 ± 0.16	3.20 ± 1.36
MMSE at baseline	29.09 ± 1.19	27.09 ± 1.82**	26.81 ± 2.22**
MMSE at first follow-up	29.16 ± 1.16	27.02 ± 1.72**	25.74 ± 1.59**##
MMSE at second follow-up	28.99 ± 1.05	26.54 ± 2.19**	23.67 ± 2.83**##
ADAS at baseline	8.03 ± 4.26	16.07 ± 7.30**	16.43 ± 7.81**
ADAS at first follow-up	8.52 ± 4.67	16.58 ± 5.94**	19.45 ± 6.98**#
ADAS at second follow-up	8.82 ± 4.52	17.09 ± 6.32**	26.75 ± 8.69**##

Note: Data are represented as mean ± SD. Post-hoc comparisons detected significant difference between CN and sMCI or CN and pMCI with **p < .001, between sMCI and pMCI with #p < .01 and ##p < .001.
Abbreviations: ADAS, Alzheimer's Disease Assessment Scale; MMSE, Mini Mental State Examination.

TABLE 3 Baseline WMH burden in CN, sMCI and pMCI.

		WMH burden group		
	Normalized WMH volume (%)	Small (#subject)	Medium (#subject)	Large (#subject)
CN	0.44 ± 0.50	61	22	8
sMCI	0.55 ± 0.57	54	25	11
pMCI	0.66 ± 0.62	21	15	8
p Value	.11	.28		

frontal gyrus (PHG-SFG), orbital gyrus (PHG-OrG), and lateral occipital cortex (PHG-LOcC) after correcting for multiple comparisons. Significant larger proportions of individuals in pMCI group suffered from progressive disconnections in PHG-SFG and PHG-OrG both at the first (36.36% in PHG-SFG, 52.27% in PHG-OrG) and second follow-up (59.09% in PHG-SFG, 75.00% in PHG-OrG) compared with sMCI and CN, as shown in Figure 4c,d. We also detected significant disconnectome progress located in PHG-LOcC at the second follow-up in pMCI cohorts, as shown in Figure 4b. Especially, sMCI did not differ from CN in progressive disconnections associated with parahippocampal gyrus in this longitudinal investigation. WMH-related disconnectome progress was also detected in connection between hippocampus and cingulate gyrus (Hippo-CG) as shown in Figure 5a. In pMCI group, 9.09% and 20.45% individuals underwent progressive disconnections at the first and second follow-up, which were significantly higher than sMCI and CN (Figure 5b). At the first follow-up, no subject suffered from this disconnectome progress both in sMCI and CN groups. At the second follow-up, the proportion of sMCI patients with progressive disconnection happened in Hippo-CG had increased from 0.00% to 7.78%, which differed themselves from CN cohorts with p < .05. This disconnectome progress pattern at Hippo-CG had survived multiple comparison correction both at the first and second follow-up.

3.4 | Prediction models for conversion from MCI to AD

As shown in Table 4, the best performance based on all four metrics (accuracy, AUC, sensitivity and specificity) at baseline was achieved by model SVM-2 using node disconnectome as features. At the first follow-up, model RF-4 had achieved best performance based on mean accuracy (0.82) and specificity (0.82). SVM-4 achieved highest mean sensitivity (0.86), and highest mean AUC (0.91). Furthermore, at both baseline and the first follow-up, models using node disconnectome or node disconnectome progress as features had better performance compared with models using WMH volumes as features no matter which classification algorithm was employed, most of them had achieved significant improvements based on accuracy, AUC, sensitivity and specificity. The mean ROC under 100 times of cross-validation were presented in Figures S1–S3.

4 | DISCUSSION

In this study, we used an atlas-guided indirect mapping framework to detect WMH-related spatial–temporal progressive brain structural disconnectome across AD spectrum. The baseline brain disconnectome differed among CN, sMCI, and pMCI in connectivity between

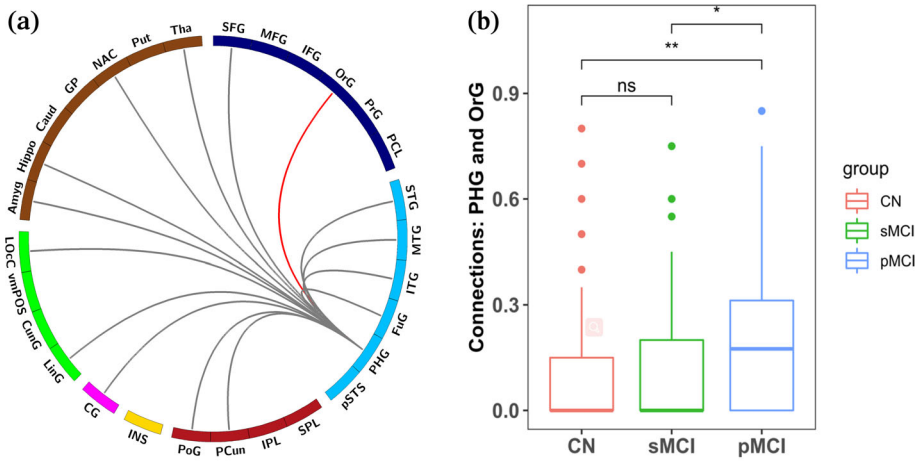

FIGURE 3 WMH-related parcel-wise disconnectome at baseline. Significant group differences were detected in connections between parahippocampal gyrus (PHG) and orbital gyyrus (OrG) after correcting for multiple comparisons. (a) Structural connections between PHG and other cerebral gray matter regions are shown by chord chart. Red link indicates significant group difference was detected on this connection. (b) Post hoc comparison results are shown with: $^{*}p < .05$; $^{**}p < .01$. ns, no significance.

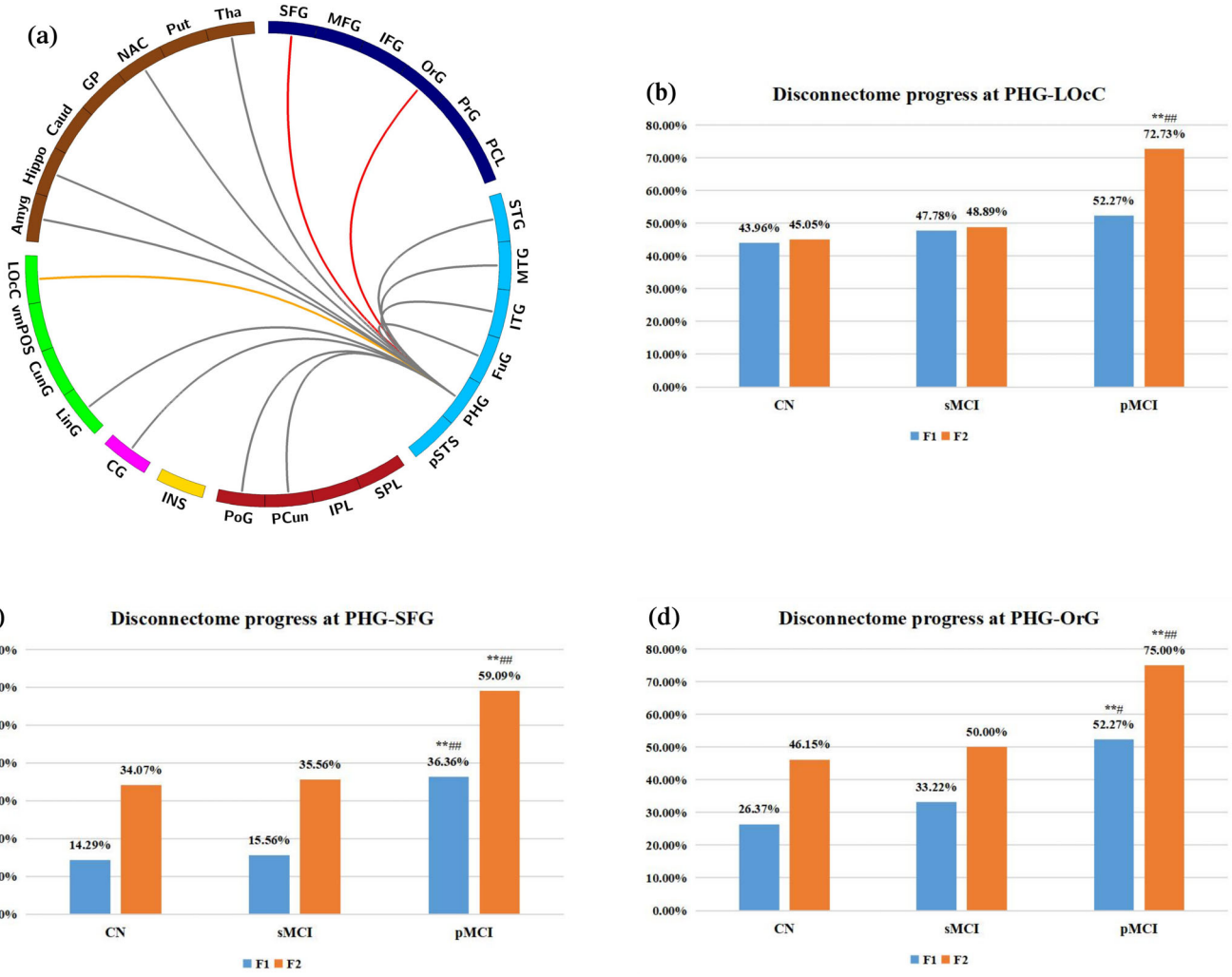

FIGURE 4 WMH-related disconnectome progress was detected in connections associated with parahippocampal gyrus. (a) Structural connections between parahippocampal gyrus and other cerebral gray matter regions are shown by chord chart. Red link indicates that group difference of disconnectome progress was detected within specific connectivity both at the first and second follow-up after correcting for multiple comparisons. Gold link denotes that group difference was only detected at the second follow-up after correcting for multiple comparisons. Proportions of subjects suffering from progressive disconnections between PHG and (b) LOcC, (c) SFG, and (d) OrG are shown. PHG, parahippocampal gyrus; SFG, superior frontal gyrus; OrG, orbital gyrus; LOcC, lateral occipital cortex. Abbreviations for other brain regions are shown in Appendix. F1, the first follow-up; F2, the second follow-up. Post hoc analysis was performed with $^{**}p < .01$ compared with CN; $\#p < .05$, and $\#\#p < .01$ compared with sMCI.

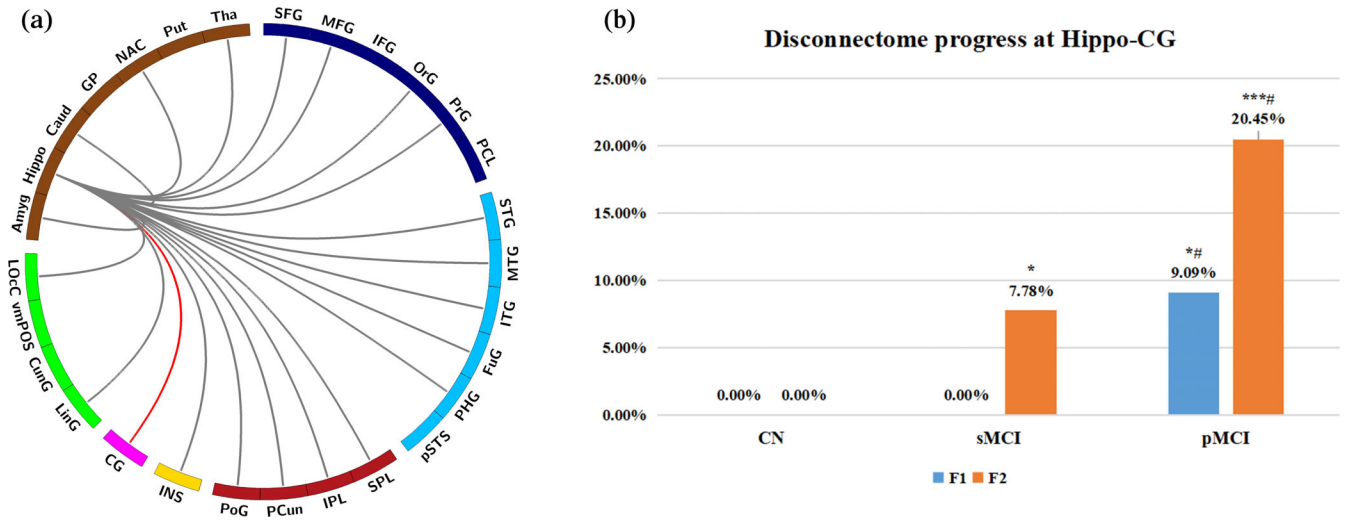

FIGURE 5 WMH-related disconnectome progress was detected in connections between hippocampus and cingulate gyrus. Structural connections between (a) hippocampus and other cerebral gray matter regions are shown by chord chart. Red link indicates that group difference of disconnectome progress was detected both at the first and second follow-up after correcting for multiple comparisons. (b) Proportions of subjects in three groups suffering from progressive disconnections are shown. Hippo, hippocampus; CG, cingulate gyrus. Abbreviations for other brain regions are shown in Appendix. F1, the first follow-up; F2, the second follow-up. Post hoc analysis was performed with, $*p < .05$, and $***p < .001$ compared with CN; $\#p < .05$ compared with sMCI.

TABLE 4 Performance of prediction models for conversion from MCI to dementia.

Model-ID	Visit	Feature	Accuracy	AUC	Sensitivity	Specificity
LR-1	BL	vols	0.67 ± 0.18	0.71 ± 0.15	0.67 ± 0.09	0.68 ± 0.10
LR-2	BL	disconnectome	0.72 ± 0.13*	0.84 ± 0.16**	0.73 ± 0.11**	0.71 ± 0.19
LR-3	F1	vols	0.66 ± 0.12	0.72 ± 0.14	0.70 ± 0.11	0.61 ± 0.10
LR-4	F1	disconnectome	0.78 ± 0.16**	0.86 ± 0.12**	0.78 ± 0.16**	0.78 ± 0.15**
LR-5	F1	DP	0.74 ± 0.19**	0.76 ± 0.13*	0.77 ± 0.17**	0.70 ± 0.17**
SVM-1	BL	vols	0.67 ± 0.14	0.81 ± 0.16	0.65 ± 0.13	0.70 ± 0.12
SVM-2	BL	disconnectome	**0.74 ± 0.17****	**0.86 ± 0.10****	**0.74 ± 0.21****	**0.74 ± 0.19***
SVM-3	F1	vols	0.72 ± 0.17	0.83 ± 0.13	0.75 ± 0.14	0.69 ± 0.20
SVM-4	F1	disconnectome	0.81 ± 0.10**	**0.91 ± 0.08****	**0.86 ± 0.16****	0.77 ± 0.18**
SVM-5	F1	DP	0.79 ± 0.13**	0.90 ± 0.08**	0.82 ± 0.11**	0.77 ± 0.10**
RF-1	BL	vols	0.68 ± 0.21	0.72 ± 0.19	0.67 ± 0.14	0.71 ± 0.15
RF-2	BL	disconnectome	0.73 ± 0.20*	0.74 ± 0.17	0.73 ± 0.22*	0.73 ± 0.20
RF-3	F1	vols	0.70 ± 0.15	0.72 ± 0.17	0.73 ± 0.16	0.68 ± 0.18
RF-4	F1	disconnectome	**0.82 ± 0.14****	0.80 ± 0.14**	0.82 ± 0.12**	**0.82 ± 0.12****
RF-5	F1	DP	0.79 ± 0.11**	0.86 ± 0.10**	0.77 ± 0.13*	0.82 ± 0.13**

Note: $*p < .05$ or $**p < .01$ compared with prediction model utilizing normalized regional WMH volumes as features at the same visit. Bold-face indicates best performance at baseline or the first follow-up.

Abbreviations: BL, baseline; disconnectome, node disconnectome; DP, node disconnectome progress; F1, the first follow-up; LR, logistic regression; RF, random forest; SVM, support vector machine; vols, regional WMH volumes.

orbital gyrus and parahippocampal gyrus. We then located the temporal progressive disconnectome patterns within connectivity associated with parahippocampal gyrus and hippocampus. Using features associated with brain disconnectome, our best prediction models achieved mean accuracy of 0.82, mean sensitivity of 0.86, mean specificity of 0.82 and mean AUC of 0.91 at average of 2.06 years before conversion, which had outperformed models using lesion volumes as predictors in this study.

4.1 | Atlas-based indirect mapping of brain structural disconnectome

WMH-related disconnectome hypothesis states that WMHs might give rise to clinical symptoms through its effects on structure or functional connected brain networks (C. D. Langen et al., 2018; Carolyn D. Langen et al., 2017; Ter Telgte et al., 2018). Mounting evidence have confirmed that associations between the presence of WMHs

and decreased cognitive functions were, at least in part, mediated through network disruption (Ter Telgte et al., 2018; Tuladhar et al., 2017; Wardlaw et al., 2019). These results have supported our hypothesis that WMHs contribute to AD related neurodegeneration and dementia by producing progressive impairments within brain structural connectivity. In this paper, we proposed a computation framework which can monitor the spatial–temporal progression of individual brain disconnectome at parcel-wise connection level. The main challenge for detecting WMH-related disconnectome is that lesions can alter the diffusion properties of white matter and disrupt computerized fiber tracking algorithms (Griffis et al., 2021). In order to tackle this problem, virtual lesion method (Griffis et al., 2021; Li et al., 2021) had been proposed by conducting fiber tracking using DTI from healthy subjects with white matter lesions inserted as regions of avoidance after coregistration. This method has also been termed as indirect mapping (Salvalaggio et al., 2020). In our study, we also used indirect mapping to characterize the location of WMHs within parcel-wise brain connectivity. Brain disconnectome were normalized by atlas connectome: "HCP842" (Yeh et al., 2018), which enabled the evaluation of disconnection severity for individual subject.

4.2 | Patterns of WMH-related structural disconnectome in AD

Alzheimer's disease is increasingly considered as a progressive degenerative disease, associated with the aggregation of heterogeneous pathologies, including pathological proteins, cortical atrophy, metabolic dysfunction, cerebrovascular alterations and so on (Dubois et al., 2021; Sweeney et al., 2019). These pathological changes are posited to arise in a stereotypical spatial–temporal manner, which targeting intrinsic structural and functional brain networks in the brain, and eventually induced primary amnestic syndrome and other domains of cognitive impairments (Mito et al., 2018).

Mounting evidences demonstrate that a stereotypical distribution of white matter degeneration exists in patients on the continuum of AD progression (Mak et al., 2017; Mito et al., 2018; Pichet Binette et al., 2021), evident in specific fiber pathways including the cingulum bundle along its anterior, posterior, and parahippocampal aspects, the splenium and genu corpus callosum, uncinate fasciculus, inferior fronto-occipital fasciculus, the inferior longitudinal fasciculus and arcuate fasciculus (Chen et al., 2020; Kitamura et al., 2013; Luo et al., 2020; Mito et al., 2018). These fiber pathways are majorly associated with default mode network (DMN) nodes, which is most notably attacked by AD pathologies as confirmed by studies using functional neuroimaging (Brier et al., 2014; Jones et al., 2015; Jones et al., 2017). In our results, we had detected spatial–temporal progressive structural disconnectome located in connections between PHG and SFG, PHG and OrG, which belong to uncinate fasciculus (Catani et al., 2002). Uncinate fasciculus connects the orbitofrontal cortex with temporal lobe, which has been proposed that it plays a role in verbal and semantic performance (Han et al., 2013). Connection between PHG and LOcG belong to inferior longitudinal fasciculus (Catani et al., 2002), theses fiber tracts are critically involved in visually guided behaviors (Zemmoura et al., 2021). Connection between Hippo and CG is part of parahippocampal cingulum (Bubb et al., 2018), which is strongly associated with episodic memory (Bubb et al., 2018). The spatial–temporal progressive patterns we found are in line with the stereotypical distribution of white matter degeneration in AD progression detected by previous studies.

Although the impairments of white matter microstructure is commonly considered a key marker both in AD and CSVD, recent studies conclude that in memory clinical patients, the effect of CSVD on diffusion alterations of brain structural connectivity is largely exceeds the effect of AD (Dewenter et al., 2022; Finsterwalder et al., 2020). Taylor et al. suggested that degeneration of fiber pathway may be closely related to vascular pathology and WMHs, most evident in tracts connecting the brain regions in DMN (Taylor et al., 2016). However, previous researches did not associate the structural connectivity with the presence of WMHs, such that the contribution of CSVD to the AD-related white matter degeneration was not fully considered. In our study, we used indirect mapping to associate the regional WMH lesions to parcel-wise connection by spatially mapping, which to our knowledge, is the first study hammering at assessing the spatial–temporal patterns of WMH-related structural disconnectivity across AD spectrum by a longitudinal investigation. Our results seem to indicate that the stereotypical distribution pattern of white matter degeneration in AD is largely determined by the regional accumulation of WMHs.

AD pathologies (tau and amyloid-β) target distinctive brain connectivity in aging brain, involving different subregions of medial temporal lobe (Dautricourt et al., 2021; Maass et al., 2019). Anterior temporal (AT) and posterior medial (PM) networks are selectively vulnerable to AD pathologies in cognitively normal elderly subjects, with tau targeting the AT network, whereas amyloid-β pathology preferentially affects the PM network (Guzmán-Vélez et al., 2022; Maass et al., 2019). In this paper, we had also located distinctive and progressive spatial–temporal WMH-related disconnectome patterns within connectivity arising from MTL (PHG and Hippo) to important nodes belonging to AT (SFG and OrG) and PM (LoCG) network. Furthermore, the vascular two-hit hypothesis of AD pathophysiology proposed that: a synergistic relationship exists between the vascular dysfunction (hit one) and amyloid-β accumulation (hit two) and hyperphosphorylation of tau, which initially forms in the medial temporal lobe and hippocampus during the early stages AD before progressing to neocortex (Braak & Braak, 1996; Iturria-Medina et al., 2016; Sweeney et al., 2019). As shown in our results, in progressive MCI group, vascular origin WMHs preferentially attacked specific brain connectivity, which is also vulnerable to amyloid-β plaques and tau neurofibrillary tangles. These results supported the important role of vascular dysfunction in AD pathophysiology proposed by two-hit hypothesis. We had located the vulnerable neural circuits related to the progression of regional WMHs in patients on the AD continuum, this might aid in developing screening method for early prodromal patients and future therapies targeting in intervening vascular dysfunction in AD.

4.3 | Brain disconnectome as predictor for AD progress

The neurodegenerative process associated with AD leads to profound structural and functional changes in the brain. In classification between sMCI and pMCI, several studies achieved accuracy of 72.41%–81.50% using tissue density maps, cortical surface and structural texture of predefined ROIs as features with data enrolled from ADNI (Liu, Zhang, Shen, & Alzheimer's Disease Neuroimaging, 2015; Min et al., 2014; Misra et al., 2009; Sørensen et al., 2016). Using fluorodeoxyglucose positron-emission tomography (FDG-PET) to measure the alterations in brain metabolism, Cabral et al. achieved mean accuracy of 74%–86% for the classification between sMCI and different sets of pMCI subjects, which were divided based on their time to conversion from 24 months to 6 months (Cabral et al., 2015). SVM, RF, LR and LDA were commonly used learning algorithms (Rathore et al., 2017).

In the past decade, deep-learning based approach have gained considerable attention in early detection and automated classification of AD, as it has powerful ability to process high dimensional multimodal neuroimaging-based features and other heterogeneous biomarkers. The combination of traditional machine learning for classification and stacked auto-encoder (SAE) for feature selection produced accuracy up to 83.3% for prediction of conversion from mild cognitive impairment (MCI) (Suk et al., 2015). Deep learning approaches, such as convolutional neural network (CNN) or recurrent neural network (RNN), that use neuroimaging data without preprocessing for feature selection have yielded accuracies up to 84.2% for MCI conversion prediction (Choi, Jin, & Alzheimer's Disease Neuroimaging, 2018). The best classification performance was obtained when multimodal neuroimaging, flurodeoxyglucose and florbetapir PET and fluid biomarkers were combined (Jo et al., 2019).

Recently, Valentina Bordin et al. explored the problem of "Explainable AI" in AD classification tasks using occlusion sensitivity method, their results revealed a promisingly relevant contribution of the WMH regions in the classification task of AD diagnose and prognosis (Bordin et al., 2022). Moreover, Yun Wang et al. used brain morphometry and white matter connectomes to formulate diagnose and prognosis models for AD (Wang et al., 2019). The white matter connectomes were constructed by probabilistic tractography using constrained spherical devolution, streamline counts and mean length were used as connectivity metrics. Benchmark models used regional WMH volumes and CSF biomarkers as features (Wang et al., 2019). The results showed that in predicting MCI to AD progression in a smaller cohort of ADNI-2 ($n = 60$), the morphometry and connectome model showed performance with 69% accuracy compared with benchmark model with 70% accuracy (Wang et al., 2019). However, their prediction models did not associated structural connectome with the presence of WMHs.

Given our goal is to evaluate the WMH-related brain structural disconnectome as a promising predictor for conversion from MCI to dementia, rather than to find a novel machine learning algorithm. We formulated our classification models using random forest, logistic regression and support vector machine, which were extensively used in the literature (Rathore et al., 2017). We also want to prove that WMH-related brain disconnectome is a better image marker in predicting AD-related neurodegeneration compared with WMH volumes. Thus we compared model performances utilizing different features consisted of normalized regional WMH volumes, node disconnnectome and node disconnectome progress. Our results (Table 4) showed that all the models using disconnectome-related features had outperformed those using lesion volume-related features at both baseline and the first follow-up. Our models using disconnectome had achieved accuracies of classification between sMCI and pMCI up to 74%–82% at the first follow-up, which is on average 2.06 years before connversion. This result is comparable to previous studies utilizing structural MRI or connectome-based image markers with traditional machine learning algorithms as classification models (Rathore et al., 2017; Sørensen et al., 2016; Wang et al., 2019). Although using deep learning-based methods along with multimodal neuroimaging, especially with FDG-PET and amyloid-PET, higher accuracies for predicting conversion can be achieved (Cabral et al., 2015; Jo et al., 2019; Ottoy et al., 2019), we had proved in this study that WMH-related brain structural disconnnectome is a promising image marker for AD progression.

4.4 | Limitations and future directions

Several limitations of this study should be noted. First, we only enrolled 44 subjects in pMCI group in this study, which is a small dataset for lesion-symptom mapping studies. Larger and multicenter datasets are needed for further investigation. Second, most of the subjects in our study underwent three visits during 3–5 years, in subjects with progressive cognitive deficit, a longer and more frequent visits for assessing neuroimaging and clinical evaluation should benefit longitudinal lesion-symptom mapping studies. Last, we used indirect mapping to characterize the location of WMHs within specific parcel-wise brain connectivity. In this case, fiber tracking was performed in other healthy subjects to compute an atlas for lesion mapping, thus we did not unravel how the presence of WMHs affect the diffusion properties of the traversed fiber tracts. Methods of building brain connectivity directly in cohorts with heavy WMH burden are important for further investigation.

5 | CONCLUSION

We used an atlas-guided indirect mapping framework to detect WMH-related spatial–temporal progressive brain structural disconnectome during AD neurodegeneration process. Our results found that connections between: (1) parahippocampal gyrus and superior frontal gyrus, orbital gyrus, and lateral occipital cortex; and (2) hippocampus and cingulate gyrus are vulnerable to the attack of regional WMHs in patients on the AD continuum. By developing and

evaluating prediction models, we further showed that WMH-related brain structural disconnectome can be used as promising predictor for conversion from MCI to dementia. These results indicated that a synergistic relationship exists between multiple contributors of AD: cerebral small vessel, amyloid-β accumulation and hyperphosphorylation of tau, as they attack similar brain connections at the early stage of AD.

AUTHOR CONTRIBUTIONS

Li Liang, Qi Yang and Ting Ma contributed to the conception and design of this study. Li Liang contributed to data analysis, brain disconnectome computing and statistical modeling. Pengzheng Zhou and Chenfei Ye contributed to quality control associated with WMH segmentation, MRI processing and visualization. Li Liang and Ting Ma contributed to drafting and revising the manuscript.

ACKNOWLEDGMENTS

This study is by grants from the National Natural Science Foundation of China (62276081, 62106113), the Innovation Team and Talents Cultivation Program of National Administration of Traditional Chinese Medicine (NO: ZYYCXTD-C-202004), Basic Research Foundation of Shenzhen Science and Technology Stable Support Program (GXWD20201230155427003-20200822115709001). We thanks the Alzheimer's Disease Neuroimaging Initiative (ADNI) database (adni.loni.usc.edu) as the neuroimaging, demographics, diagnostic and neuropsychological scale information were all collected from this database. The ADNI was launched in 2003 by the National Institute on Aging (NIA), the National Institute of Biomedical Imaging and Bioengineering (NIBIB), the Food and Drug Administration (FDA), private pharmaceutical companies and non-profit organisations, as a public-private partnership. The goal of the ADNI study is to track the progression of the disease using biomarkers, together with clinical measures, to assess the alterations of brain structure and function over the course of AD progression.

CONFLICT OF INTEREST STATEMENT

The authors declare no conflict of interest.

DATA AVAILABILITY STATEMENT

Data supporting the findings of this study were enrolled from ADNI database, which are available from the corresponding author on request.

ORCID

Li Liang https://orcid.org/0000-0003-3479-1229
Ting Ma https://orcid.org/0000-0001-8819-6228

REFERENCES

Apátiga-Pérez, R., Soto-Rojas, L. O., Campa-Córdoba, B. B., Luna-Viramontes, N. I., Cuevas, E., Villanueva-Fierro, I., Ontiveros-Torres, M. A., Bravo-Muñoz, M., Flores-Rodríguez, P., Garcés-Ramirez, L., de la Cruz, F., Montiel-Sosa, J. F., Pacheco-Herrero, M., & Luna-Muñoz, J. (2021). Neurovascular dysfunction and vascular amyloid accumulation as early events in Alzheimer's disease. *Metabolic Brain Disease*, *37*(1), 39–50. https://doi.org/10.1007/s11011-021-00814-4

Avants, B. B., Epstein, C. L., Grossman, M., & Gee, J. C. (2008). Symmetric diffeomorphic image registration with cross-correlation: Evaluating automated labeling of elderly and neurodegenerative brain. *Medical Image Analysis*, *12*(1), 26–41. https://doi.org/10.1016/j.media.2007.06.004

Benjamini, Y., & Hochberg, Y. (1995). Controlling the false discovery rate: A practical and powerful approach to multiple testing. *Journal of the Royal statistical society: series B (Methodological)*, *57*(1), 289–300.

Bordin, V., Coluzzi, D., Rivolta, M. W., & Baselli, G. (2022). Explainable AI points to white matter hyperintensities for Alzheimer's disease identification: A preliminary study. *Annual International Conference of the IEEE Engineering in Medicine and Biology Society*, *2022*, 484–487. https://doi.org/10.1109/embc48229.2022.9871306

Braak, H., & Braak, E. (1996). Evolution of the neuropathology of Alzheimer's disease. *Acta Neurologica Scandinavica. Supplementum*, *165*, 3–12. https://doi.org/10.1111/j.1600-0404.1996.tb05866.x

Brier, M. R., Thomas, J. B., & Ances, B. M. (2014). Network dysfunction in Alzheimer's disease: Refining the disconnection hypothesis. *Brain Connectivity*, *4*(5), 299–311. https://doi.org/10.1089/brain.2014.0236

Bubb, E. J., Metzler-Baddeley, C., & Aggleton, J. P. (2018). The cingulum bundle: Anatomy, function, and dysfunction. *Neuroscience and Biobehavioral Reviews*, *92*, 104–127. https://doi.org/10.1016/j.neubiorev.2018.05.008

Cabral, C., Morgado, P. M., Campos Costa, D., & Silveira, M. (2015). Predicting conversion from MCI to AD with FDG-PET brain images at different prodromal stages. *Computers in Biology and Medicine*, *58*, 101–109. https://doi.org/10.1016/j.compbiomed.2015.01.003

Catani, M., Howard, R. J., Pajevic, S., & Jones, D. K. (2002). Virtual in vivo interactive dissection of white matter fasciculi in the human brain. *NeuroImage*, *17*(1), 77–94. https://doi.org/10.1006/nimg.2002.1136

Chen, H., Huang, L., Li, H., Qian, Y., Yang, D., Qing, Z., Luo, C., Li, M., Zhang, B., & Xu, Y. (2020). Microstructural disruption of the right inferior fronto-occipital and inferior longitudinal fasciculus contributes to WMH-related cognitive impairment. *CNS Neuroscience & Therapeutics*, *26*(5), 576–588. https://doi.org/10.1111/cns.13283

Choi, H., Jin, K. H., & Alzheimer's Disease Neuroimaging Initiative. (2018). Predicting cognitive decline with deep learning of brain metabolism and amyloid imaging. *Behavioural Brain Research*, *344*, 103–109. https://doi.org/10.1016/j.bbr.2018.02.017

Dadar, M., Camicioli, R., Duchesne, S., & Collins, D. L. (2020). The temporal relationships between white matter hyperintensities, neurodegeneration, amyloid beta, and cognition. *Alzheimers Dementia (Amsterdam)*, *12*(1), e12091. https://doi.org/10.1002/dad2.12091

Dautricourt, S., Flores, R., Landeau, B., Poisnel, G., Vanhoutte, M., Delcroix, N., Eustache, F., Vivien, D., Sayette, V., & Chételat, G. (2021). Longitudinal changes in hippocampal network connectivity in alzheimer's disease. *Annals of Neurology*, *90*(3), 391–406. https://doi.org/10.1002/ana.26168

Dewenter, A., Jacob, M. A., Cai, M., Gesierich, B., Hager, P., Kopczak, A., Biel, D., Ewers, M., Tuladhar, A. M., de Leeuw, F.-E., Dichgans, M., Franzmeier, N., & Duering, M. (2022). Disentangling the effects of Alzheimer's and small vessel disease on white matter fibre tracts. *Brain*, *146*(2), 678–689. https://doi.org/10.1093/brain/awac265

Dhollander, T., Clemente, A., Singh, M., Boonstra, F., Civier, O., Duque, J. D., Egorova, N., Enticott, P., Fuelscher, I., Gajamange, S., Genc, S., Gottlieb, E., Hyde, C., Imms, P., Kelly, C., Kirkovski, M., Kolbe, S., Liang, X., Malhotra, A., … Caeyenberghs, K. (2021). Fixel-based analysis of diffusion mri: methods, applications. *Challenges and Opportunities. Neuro Image*, *241*, 118417. https://doi.org/10.1016/j.neuroimage.2021.118417

Dubois, B., Villain, N., Frisoni, G. B., Rabinovici, G. D., Sabbagh, M., Cappa, S., Bejanin, A., Bombois, S., Epelbaum, S., Teichmann, M., Habert, M.-O., Nordberg, A., Blennow, K., Galasko, D., Stern, Y., Rowe, C. C., Salloway, S., Schneider, L. S., Cummings, J. L., & Feldman, H. H. (2021). Clinical diagnosis of Alzheimer's disease: recommendations of the International

Working Group. *The Lancet Neurology*, *20*(6), 484–496. https://doi.org/10.1016/s1474-4422(21)00066-1

Dukart, J., Schroeter, M. L., & Mueller, K. (2011). Age correction in dementia—Matching to a healthy brain. *PLoS One*, *6*(7), e22193. https://doi.org/10.1371/journal.pone.0022193

Fan, L., Li, H., Zhuo, J., Zhang, Y., Wang, J., Chen, L., Yang, Z., Chu, C., Xie, S., Laird, A. R., Fox, P. T., Eickhoff, S. B., Yu, C., & Jiang, T. (2016). The human brainnetome atlas: a new brain atlas based on connectional architecture. *Cerebral Cortex*, *26*(8), 3508–3526. https://doi.org/10.1093/cercor/bhw157

Finsterwalder, S., Vlegels, N., Gesierich, B., Araque Caballero, M. Á., Weaver, N. A., Franzmeier, N., Georgakis, M. K., Konieczny, M. J., Koek, H. L., Karch, C. M., Graff-Radford, N. R., Salloway, S., Oh, H., Allegri, R. F., Chhatwal, J. P., Jessen, F., Düzel, E., Dobisch, L., … Metzger, C. (2020). Small vessel disease more than Alzheimer's disease determines diffusion MRI alterations in memory clinic patients. *Alzheimer's & Dementia*, *16*(11), 1504–1514. https://doi.org/10.1002/alz.12150

Griffis, J. C., Metcalf, N. V., Corbetta, M., & Shulman, G. L. (2021). Lesion quantification toolkit: A MATLAB software tool for estimating grey matter damage and white matter disconnections in patients with focal brain lesions. *NeuroImage: Clinical*, *30*, 102639. https://doi.org/10.1016/j.nicl.2021.102639

Guzmán-Vélez, E., Diez, I., Schoemaker, D., Pardilla-Delgado, E., Vila-Castelar, C., Fox-Fuller, J. T., Baena, A., Sperling, R. A., Johnson, K. A., Lopera, F., Sepulcre, J., & Quiroz, Y. T. (2022). Amyloid-β and tau pathologies relate to distinctive brain dysconnectomics in preclinical autosomal-dominant Alzheimer's disease. *Proceedings of the National Academy of Sciences*, *119*(15), e2113641119. https://doi.org/10.1073/pnas.2113641119

Han, Z., Ma, Y., Gong, G., He, Y., Caramazza, A., & Bi, Y. (2013). White matter structural connectivity underlying semantic processing: Evidence from brain damaged patients. *Brain*, *136*(Pt 10), 2952–2965. https://doi.org/10.1093/brain/awt205

Hu, H.-Y., Ou, Y.-N., Shen, X.-N., Qu, Y., Ma, Y.-H., Wang, Z.-T., Dong, Q., Tan, L., & Yu, J.-T. (2021). White matter hyperintensities and risks of cognitive impairment and dementia: A systematic review and meta-analysis of 36 prospective studies. *Neuroscience and Biobehavioral Reviews*, *120*, 16–27. https://doi.org/10.1016/j.neubiorev.2020.11.007

Iadecola, C. (2017). The neurovascular unit coming of age: A journey through neurovascular coupling in health and disease. *Neuron*, *96*(1), 17–42. https://doi.org/10.1016/j.neuron.2017.07.030

Iturria-Medina, Y., Sotero, R. C., Toussaint, P. J., Mateos-Pérez, J. M., Evans, A. C., Weiner, M. W., Aisen, P., Petersen, R., Jack, C. R., Jagust, W., Trojanowki, J. Q., Toga, A. W., Beckett, L., Green, R. C., Saykin, A. J., Morris, J., Shaw, L. M., Khachaturian, Z., … Sorensen, G. (2016). Early role of vascular dysregulation on late-onset Alzheimer's disease based on multifactorial data-driven analysis. *Nature Communications*, *7*(1), 11934. https://doi.org/10.1038/ncomms11934

Jenkinson, M., Bannister, P., Brady, M., & Smith, S. (2002). Improved optimization for the robust and accurate linear registration and motion correction of brain images. *NeuroImage*, *17*(2), 825–841. https://doi.org/10.1006/nimg.2002.1132

Jenkinson, M., & Smith, S. (2001). A global optimisation method for robust affine registration of brain images. *Medical Image Analysis*, *5*(2), 143–156. https://doi.org/10.1016/s1361-8415(01)00036-6

Jo, T., Nho, K., & Saykin, A. J. (2019). Deep learning in Alzheimer's disease: Diagnostic classification and prognostic prediction using Neuroimaging data. *Frontiers in Aging Neuroscience*, *11*, 220. https://doi.org/10.3389/fnagi.2019.00220

Jones, D. T., Graff-Radford, J., Lowe, V. J., Wiste, H. J., Gunter, J. L., Senjem, M. L., Botha, H., Kantarci, K., Boeve, B. F., Knopman, D. S., Petersen, R. C., & Jack, C. R. (2017). Tau, amyloid, and cascading network failure across the Alzheimer's disease spectrum. *Cortex*, *97*, 143–159. https://doi.org/10.1016/j.cortex.2017.09.018

Jones, D. T., Knopman, D. S., Gunter, J. L., Graff-Radford, J., Vemuri, P., Boeve, B. F., Petersen, R. C., Weiner, M. W., & Jack, C. R. (2015). Cascading network failure across the Alzheimer's disease spectrum. *Brain*, *139*(2), 547–562. https://doi.org/10.1093/brain/awv338

Joutel, A., & Chabriat, H. (2017). Pathogenesis of white matter changes in cerebral small vessel diseases: Beyond vessel-intrinsic mechanisms. *Clinical Science (London, England)*, *131*(8), 635–651. https://doi.org/10.1042/cs20160380

Kapasi, A., DeCarli, C., & Schneider, J. A. (2017). Impact of multiple pathologies on the threshold for clinically overt dementia. *Acta Neuropathologica*, *134*(2), 171–186. https://doi.org/10.1007/s00401-017-1717-7

Kitamura, S., Kiuchi, K., Taoka, T., Hashimoto, K., Ueda, S., Yasuno, F., Morikawa, M., Kichikawa, K., & Kishimoto, T. (2013). Longitudinal white matter changes in Alzheimer's disease: A tractography-based analysis study. *Brain Research*, *1515*, 12–18. https://doi.org/10.1016/j.brainres.2013.03.052

Langen, C. D., Cremers, L. G. M., de Groot, M., White, T., Ikram, M. A., Niessen, W. J., & Vernooij, M. W. (2018). Disconnection due to white matter hyperintensities is associated with lower cognitive scores. *NeuroImage*, *183*, 745–756. https://doi.org/10.1016/j.neuroimage.2018.08.037

Langen, C. D., Vernooij, M. W., Cremers, L. G. M., Huizinga, W., de Groot, M., Ikram, M. A., White, T., & Niessen, W. J. (2017). The structural disconnectome: A pathology-sensitive extension of the structural connectome. In *2017 IEEE 14th International Symposium on Biomedical Imaging*, (ISBI 2017). https://doi.org/10.1109/isbi.2017.7950539

Li, Z., Dolui, S., Habes, M., Bassett, D. S., Wolk, D., & Detre, J. A. (2021). Predicted disconnectome associated with progressive periventricular white matter ischemia. *Cerebral Circulation Cognition & Behavior*, *2*, 100022. https://doi.org/10.1016/j.cccb.2021.100022

Liang, L., Zhou, P., Lu, W., Guo, X., Ye, C., Lv, H., Wang, T., & Ma, T. (2021). An anatomical knowledge-based MRI deep learning pipeline for white matter hyperintensity quantification associated with cognitive impairment. *Computerized Medical Imaging and Graphics*, *89*, 101873. https://doi.org/10.1016/j.compmedimag.2021.101873

Liu, M., Zhang, D., Shen, D., & Alzheimer's Disease Neuroimaging Initiative. (2015). View-centralized multi-atlas classification for Alzheimer's disease diagnosis. *Human Brain Mapping*, *36*(5), 1847–1865. https://doi.org/10.1002/hbm.22741

Lorenzini, L., Ansems, L. T., Lopes Alves, I., Ingala, S., Vállez García, D., Tomassen, J., Sudre, C., Salvadó, G., Shekari, M., Operto, G., Brugulat-Serrat, A., Sánchez-Benavides, G., ten Kate, M., Tijms, B., Wink, A. M., Mutsaerts, H. J. M. M., den Braber, A., Visser, P. J., … van Berckel, B. N. M. (2022). Regional associations of white matter hyperintensities and early cortical amyloid pathology. Brain. *Communications*, *4*(3), fcac150. https://doi.org/10.1093/braincomms/fcac150

Luo, C., Li, M., Qin, R., Chen, H., Huang, L., Yang, D., Ye, Q., Liu, R., Xu, Y., Zhao, H., & Bai, F. (2020). Long longitudinal tract lesion contributes to the progression of alzheimer's disease. *Frontiers in Neurology*, *11*, 503235. https://doi.org/10.3389/fneur.2020.503235

Maass, A., Berron, D., Harrison, T. M., Adams, J. N., La Joie, R., Baker, S., Mellinger, T., Bell, R. K., Swinnerton, K., Inglis, B., Rabinovici, G. D., Düzel, E., & Jagust, W. J. (2019). Alzheimer's pathology targets distinct memory networks in the ageing brain. *Brain*, *142*(8), 2492–2509. https://doi.org/10.1093/brain/awz154

Mak, E., Gabel, S., Mirette, H., Su, L., Williams, G. B., Waldman, A., Wells, K., Ritchie, K., Ritchie, C., & O'Brien, J. (2017). Structural neuroimaging in preclinical dementia: From microstructural deficits and grey matter atrophy to macroscale connectomic changes. *Ageing Research Reviews*, *35*, 250–264. https://doi.org/10.1016/j.arr.2016.10.001

Min, R., Wu, G., Cheng, J., Wang, Q., & Shen, D. (2014). Multi-atlas based representations for Alzheimer's disease diagnosis. *Human Brain Mapping*, *35*(10), 5052–5070. https://doi.org/10.1002/hbm.22531

Misra, C., Fan, Y., & Davatzikos, C. (2009). Baseline and longitudinal patterns of brain atrophy in MCI patients, and their use in prediction of short-term conversion to AD: Results from ADNI. *NeuroImage*, *44*(4), 1415–1422. https://doi.org/10.1016/j.neuroimage.2008.10.031

Mito, R., Raffelt, D., Dhollander, T., Vaughan, D. N., Tournier, J.-D., Salvado, O., Brodtmann, A., Rowe, C. C., Villemagne, V. L., & Connelly, A. (2018). Fibre-specific white matter reductions in Alzheimer's disease and mild cognitive impairment. *Brain*, *141*(3), 888–902. https://doi.org/10.1093/brain/awx355

Nasrabady, S. E., Rizvi, B., Goldman, J. E., & Brickman, A. M. (2018). White matter changes in Alzheimer's disease: A focus on myelin and oligodendrocytes. *Acta Neuropathologica Communications*, *6*(1), 22. https://doi.org/10.1186/s40478-018-0515-3

Ottoy, J., Niemantsverdriet, E., Verhaeghe, J., De Roeck, E., Struyfs, H., Somers, C., wyffels, L., Ceyssens, S., Van Mossevelde, S., Van den Bossche, T., Van Broeckhoven, C., Ribbens, A., Bjerke, M., Stroobants, S., Engelborghs, S., & Staelens, S. (2019). Association of short-term cognitive decline and MCI-to-AD dementia conversion with CSF, MRI, amyloid- and (18)F-FDG-PET imaging. *NeuroImage: Clinical*, *22*, 101771. https://doi.org/10.1016/j.nicl.2019.101771

Pichet Binette, A., Theaud, G., Rheault, F., Roy, M., Collins, D. L., Levin, J., Mori, H., Lee, J. H., Farlow, M. R., Schofield, P., Chhatwal, J. P., Masters, C. L., Benzinger, T., Morris, J., Bateman, R., Breitner, J. C., Poirier, J., Gonneaud, J., … Descoteaux, M. (2021). Bundle-specific associations between white matter microstructure and Aβ and tau pathology in preclinical Alzheimer's disease. *eLife*, *10*, e62929. CLOCKSS. https://doi.org/10.7554/elife.62929

Raghavan, S., Przybelski, S. A., Reid, R. I., Lesnick, T. G., Ramanan, V. K., Botha, H., Matchett, B. J., Murray, M. E., Reichard, R. R., Knopman, D. S., Graff-Radford, J., Jones, D. T., Lowe, V. J., Mielke, M. M., Machulda, M. M., Petersen, R. C., Kantarci, K., Whitwell, J. L., Josephs, K. A., … Vemuri, P. (2022). White matter damage due to vascular, tau, and TDP-43 pathologies and its relevance to cognition. *Acta Neuropathologica Communications*, *10*(1), 16. https://doi.org/10.1186/s40478-022-01319-6

Rathore, S., Habes, M., Iftikhar, M. A., Shacklett, A., & Davatzikos, C. (2017). A review on neuroimaging-based classification studies and associated feature extraction methods for Alzheimer's disease and its prodromal stages. *NeuroImage*, *155*, 530–548. https://doi.org/10.1016/j.neuroimage.2017.03.057

Ronneberger, O., Fischer, P., & Brox, T. (2015). U-net: Convolutional networks for biomedical image segmentation. In *Paper presented at the 18th international conference on medical image computing and computer-assisted intervention*, MICCAI 2015, October 5, 2015–October 9, 2015, Munich, Germany.

Salvalaggio, A., De Filippo De Grazia, M., Zorzi, M., Thiebaut de Schotten, M., & Corbetta, M. (2020). Post-stroke deficit prediction from lesion and indirect structural and functional disconnection. *Brain*, *143*(7), 2173–2188. https://doi.org/10.1093/brain/awaa156

Smith, S. M. (2002). Fast robust automated brain extraction. *Human Brain Mapping*, *17*(3), 143–155. https://doi.org/10.1002/hbm.10062

Sørensen, L., Igel, C., Liv Hansen, N., Osler, M., Lauritzen, M., Rostrup, E., & Nielsen, M. (2016). Early detection of Alzheimer's disease using MRI hippocampal texture. *Human Brain Mapping*, *37*(3), 1148–1161. https://doi.org/10.1002/hbm.23091

Soto-Rojas, L. O., Pacheco-Herrero, M., Martínez-Gómez, P. A., Campa-Córdoba, B. B., Apátiga-Pérez, R., Villegas-Rojas, M. M., Harrington, C. R., de la Cruz, F., Garcés-Ramírez, L., & Luna-Muñoz, J. (2021). The neurovascular unit dysfunction in alzheimer's disease. *International Journal of Molecular Sciences*, *22*(4), 2022. https://doi.org/10.3390/ijms22042022

Suk, H. I., Lee, S. W., & Shen, D. (2015). Latent feature representation with stacked auto-encoder for AD/MCI diagnosis. *Brain Structure & Function*, *220*(2), 841–859. https://doi.org/10.1007/s00429-013-0687-3

Sweeney, M. D., Montagne, A., Sagare, A. P., Nation, D. A., Schneider, L. S., Chui, H. C., Harrington, M. G., Pa, J., Law, M., Wang, D. J. J., Jacobs, R. E., Doubal, F. N., Ramirez, J., Black, S. E., Nedergaard, M., Benveniste, H., Dichgans, M., Iadecola, C., Love, S., … Zlokovic, B. V. (2019). Vascular dysfunction—The disregarded partner of Alzheimer's disease. Alzheimer's & Dementia, 15(1), 158–167. https://doi.org/10.1016/j.jalz.2018.07.222

Tang, X. Y., Oishi, K., Faria, A. V., Hillis, A. E., Albert, M. S., Mori, S., & Miller, M. I. (2013). Bayesian parameter estimation and segmentation in the multi-atlas random orbit model. *PLoS One*, *8*(6), 14. https://doi.org/10.1371/journal.pone.0065591

Taylor, A. N. W., Kambeitz-Ilankovic, L., Gesierich, B., Simon-Vermot, L., Franzmeier, N., Araque Caballero, M. Á., Müller, S., Hesheng, L., Ertl-Wagner, B., Bürger, K., Weiner, M. W., Dichgans, M., Duering, M., & Ewers, M. (2016). Tract-specific white matter hyperintensities disrupt neural network function in Alzheimer's disease. *Alzheimer's & Dementia*, *13*(3), 225–235. https://doi.org/10.1016/j.jalz.2016.06.2358

Ter Telgte, A., van Leijsen, E. M. C., Wiegertjes, K., Klijn, C. J. M., Tuladhar, A. M., & de Leeuw, F. E. (2018). Cerebral small vessel disease: From a focal to a global perspective. *Nature Reviews. Neurology*, *14*(7), 387–398. https://doi.org/10.1038/s41582-018-0014-y

Tibshirani, R. (1996). Regression shrinkage and selection via the lasso. *Journal of the Royal Statistical Society: Series B (Methodological)*, *58*(1), 267–288.

Tuladhar, A. M., Lawrence, A., Norris, D. G., Barrick, T. R., Markus, H. S., & de Leeuw, F. E. (2017). Disruption of rich club organisation in cerebral small vessel disease. *Human Brain Mapping*, *38*(4), 1751–1766. https://doi.org/10.1002/hbm.23479

Tustison, N. J., Avants, B. B., Cook, P. A., Zheng, Y. J., Egan, A., Yushkevich, P. A., & Gee, J. C. (2010). N4ITK: Improved N3 bias correction. *IEEE Transactions on Medical Imaging*, *29*(6), 1310–1320. https://doi.org/10.1109/tmi.2010.2046908

Vemuri, P., Lesnick, T. G., Knopman, D. S., Przybelski, S. A., Reid, R. I., Mielke, M. M., Graff-Radford, J., Lowe, V. J., Machulda, M. M., Petersen, R. C., & Jack, C. R. (2019). Amyloid, vascular, and resilience pathways associated with cognitive aging. *Annals of Neurology*, *86*(6), 866–877. https://doi.org/10.1002/ana.25600

Wang, Y., Xu, C., Park, J.-H., Lee, S., Stern, Y., Yoo, S., Kim, J. H., Kim, H. S., & Cha, J. (2019). Diagnosis and prognosis of Alzheimer's disease using brain morphometry and white matter connectomes. *Neuro Image: Clinical*, *23*, 101859. https://doi.org/10.1016/j.nicl.2019.101859

Wardlaw, J. M., Smith, C., & Dichgans, M. (2019). Small vessel disease: Mechanisms and clinical implications. *Lancet Neurology*, *18*(7), 684–696. https://doi.org/10.1016/S1474-4422(19)30079-1

Wu, D., Ma, T., Ceritoglu, C., Li, Y., Chotiyanonta, J., Hou, Z., Hsu, J., Xu, X., Brown, T., Miller, M. I., & Mori, S. (2016). Resource atlases for multi-atlas brain segmentations with multiple ontology levels based on T1-weighted MRI. *Neuro Image*, *125*, 120–130. https://doi.org/10.1016/j.neuroimage.2015.10.042

Yeh, F.-C., Panesar, S., Fernandes, D., Meola, A., Yoshino, M., Fernandez-Miranda, J. C., Vettel, J. M., & Verstynen, T. (2018). Population-averaged atlas of the macroscale human structural connectome and its network topology. *Neuro Image*, *178*, 57–68. https://doi.org/10.1016/j.neuroimage.2018.05.027

Zayed, A., Iturria-Medina, Y., Villringer, A., Sehm, B., & Steele, C. J. (2020). Rapid quantification of White matter disconnection in the human brain. *Annual International Conference of the IEEE Engineering in Medicine and Biology Society*, *2020*, 1701–1704. https://doi.org/10.1109/embc44109.2020.9176229

Zemmoura, I., Burkhardt, E., & Herbet, G. (2021). The inferior longitudinal fasciculus: Anatomy, function and surgical considerations. *Journal of Neurosurgical Sciences*, *65*(6), 590–604. https://doi.org/10.23736/s0390-5616.21.05391-1

SUPPORTING INFORMATION

Additional supporting information can be found online in the Supporting Information section at the end of this article.

How to cite this article: Liang, L., Zhou, P., Ye, C., Yang, Q., & Ma, T. (2023). Spatial–temporal patterns of brain disconnectome in Alzheimer's disease. *Human Brain Mapping*, *44*(11), 4272–4286. https://doi.org/10.1002/hbm.26344

APPENDIX A

A.1 | Gray matter parcellation

The parcellation template for constructing parcel-wise connectome consisted of 31 gray matter regions. Labels, region names and abbreviations are Label 1: superior frontal gyrus (SFG), label 2: middle frontal gyrus (MFG), label 3: inferior frontal gyrus (IFG), label 4: orbital gyrus (OrG), label 5: precentral gyrus (PrG), label 6: paracentral lobe (PCL). These are regions in frontal lobe. Label 7: superior temporal gyrus (STG), label 8: middle temporal gyrus (MTG), label 9: inferior temporal gyrus (ITG), label 10: fusiform gyrus (FuG), label 11: parahippocampal gyrus (PHG), label 12: posterior superior temporal sulcus (pSTS). These are regions in temporal lobe. Label 13: superior parietal lobule (SPL), label 14: inferior parietal lobule (IPL), label 15: precuneus (PCun), label 16: postcentral gyrus (PoG). These are regions in parietal lobe. Label 17: insular lobe (INS). Label 18: cingulate gyrus (CG). Label 19: lingual gyrus (LinG), label 20: cuneus gyrus (CunG), label 21: ventromedial parieto-occipital sulcus (vmPOS), label 22: lateral occipital cortex (LOcC). These are regions in occipital lobe. Label 23: amygdala (Amyg), label 24: hippocampus (Hippo), label 25: caudate nucleus (Caud), label 26: globus pallidus (GP), label 27: nucleus accumbens (NAC), label 28: putamen (Put), label 29: thalamus (Tha). These are regions of subcortical nuclei. Label 30: cerebellum gray matter, label 31: vermis. Parcellations from both hemispheres were combined to a single gray matter region.